

# Effect of Geometrical Modulation on pMTJ Magnetization Reversal

Christian Engel, Sarjoosing Goolaup, Han Kheng Teoh, and Wen Siang Lew

School of Physical and Mathematical Sciences, Nanyang Technological University, Singapore 637371

**Spin-transfer torque-magnetic random access memory (STT-MRAM) is one of the most prominent spintronic devices for replacing conventional electronic memory devices due to its extraordinary performance as it delivers fast operational speed, non-volatility, and a high-memory density. At advanced technology nodes, manufacturing process would invariably lead to bit on bit variation of STT-MRAM cell at wafer level. Here, we show that in a perpendicularly magnetized magnetic tunnel junction (MTJ), the in-plane demagnetizing tensor greatly influences the magnetization switching process of the free layer (FL). The geometrical asymmetry was introduced to induce a varying in-plane demagnetizing field. This impacts the stability of the MTJ and requires a larger anisotropy to sustain an out-of-plane magnetization state. Interestingly, a faster switching of the FL comprising the MTJ is observed. This resultant rapid switching is ascribed to the nucleation of a reversal embryo at the defect.**

**Index Terms**—Magnetic tunnel junction (MTJ), magnetization reversal, micromagnetics, perpendicular magnetic anisotropy (PMA), spin transfer torque (STT).

## I. INTRODUCTION

**T**HE scaling of current semiconductor-based CMOS memory technologies is limited by the increased power dissipation due to the increase in standby leakage current as the device size is scaled down. This has led to a renewed interest in investigating alternative cost-effective memory technologies as a replacement for CMOS. Spintronic devices, which utilize both the spin degree of freedom and electrical charge of electron, have been proposed as a strong candidate for universal memory technology. The manipulation of the magnetic state of nanostructure by electrical current has led to a number of spintronics-based devices.

Magnetic random access memory (MRAM) is one of the most promising candidates for next-generation non-volatile memory and logic devices owing to its high endurance, fast read/write speed and low-power consumption. The basic building block of the MRAM is the magnetic tunnel junction (MTJ), wherein an insulator layer is sandwiched between two magnetic layers. The relative orientation between two magnetic layers (parallel/anti-parallel) represents two bits, “0” and “1,” which can be read by tunnel magnetoresistance effect in an MTJ [1], [2]. Spin transfer torque (STT)-MRAM is attractive for replacing the static random access memory (SRAM) in L2 cache due to its ability for reducing the standby power to nearly zero by exhibiting same processing speed with same size [3], [4].

For STT-MRAM cells down to 10 nm node size, materials with large perpendicular magnetic anisotropy (PMA) constants are needed. A PMA material has to satisfy some of the key factors to be employed as a candidate for STT-MRAM. First, a high magnetocrystalline anisotropy constant  $K$  is required,

as it enables scaling while keeping the device immune to thermal fluctuation. For low-energy operations, the critical current needed for switching should be small. However, these two parameters scale inversely to each other. Different approaches have been introduced in order to minimize the writing energy of a perpendicular MTJ (pMTJ) such as thermally assisted switching or voltage-controlled switching [5]–[7].

As MTJ devices are scaled down for higher densities, the lithographic processes will inherently be reaching their limit. At wafer level, variation in the geometrical shapes of the patterned MTJ devices structure is expected. The minor changes in the aspect ratio and shape of the pMTJ cell leads to different switching processes.

The shape effect has been shown to greatly influence the reversal process in in-plane MTJ structures due to the shape-induced anisotropy. Goggle-shaped structures have been shown to precisely control the final magnetization configuration to reduce the spread of the switching threshold [8]. Due to the out-of-plane anisotropy in pMTJ, the shape effect is considered negligible. You and Kim [9] have shown that the pMTJ stack with circular shape exhibits a stable out-of-plane vortex configuration, which is an intermediate state between in-plane and out-of-plane magnetization state. The effect of the in-plane demagnetizing tensor on the reversal process of pMTJ has not been reported to our knowledge.

In this paper, we present a study on the effect of geometrical non-uniformity on the switching behavior of pMTJ devices. Three geometries are investigated: a symmetric (circular), a partial symmetric (elliptical), and an asymmetric (egg shape) cross section. We show that the in-plane demagnetizing tensor for a single layer is greater for elliptical and egg-shaped structure compared to circular structure. This significantly influences the reversal process of pMTJ structures. Furthermore, the symmetry in the circular pMTJ structure leads to a further stabilization of the out-of-plane and vortex magnetization configuration, whereas the geometrical asymmetry reduces the switching time of the pMTJ devices. The wide adoption of high volume manufacturing of STT-MRAM is currently

Manuscript received December 7, 2015; revised June 9, 2016, August 29, 2016, and February 7, 2017; accepted July 31, 2017. Date of publication August 4, 2017; date of current version November 16, 2017. Corresponding author: W. S. Lew (e-mail: wensiang@ntu.edu.sg).

Color versions of one or more of the figures in this paper are available online at <http://ieeexplore.ieee.org>.

Digital Object Identifier 10.1109/TMAG.2017.2736498

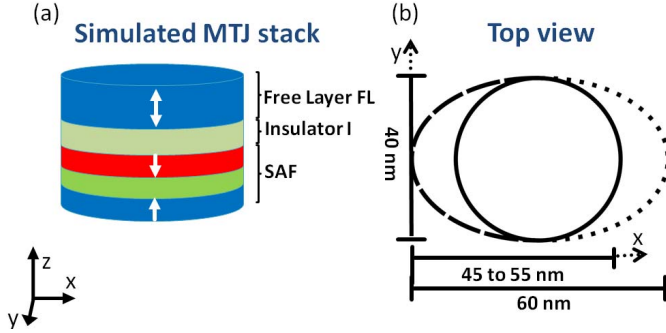


Fig. 1. (a) Schematic of the MTJ stack showing a FM for the free layer, an insulator I, and an SAF layer consisting of two FM with a non-magnetic layer NM in between. (b) Cross section of the MTJ stack is presented.

limited by the lack of a robust technology capable of patterning dense MTJ arrays. As STT-MRAM scales down, one of the requirements for MTJ patterning is to control and minimize MTJ performance degradation at small critical dimensions.

## II. MICROMAGNETIC MODEL

Micromagnetic simulations were performed using the object oriented micromagnetic framework (OOMMF) [10] which solves the augmented Landau–Lifshitz–Gilbert equation

$$\frac{d\vec{m}_s}{dt} = -\gamma \vec{m}_s \times \vec{H}_{\text{eff}} + \alpha \vec{m}_s \times \frac{d\vec{m}_s}{dt} - \gamma a_J \vec{m}_s \times (\vec{m}_s \times \vec{m}_p) - \gamma b_J (\vec{m}_s \times \vec{m}_p) \quad (1)$$

where  $\gamma$  is the gyromagnetic ratio,  $\alpha$  is the Gilbert damping constant,  $\vec{H}_{\text{eff}}$  is the effective field,  $\vec{m}_{s,p}$  is the unit vectors of the magnetization for the switching layer and polarizer layer (PL),  $a_J = a_1 J$  with  $a_1 = \varepsilon (\hbar / (2e\mu_0 M_S t))$  and  $b_J$  a second-order function of the current density  $J$ .  $\varepsilon$  is the spin polarization of the PL,  $\hbar$  is the reduced Planck's constant,  $e$  is the electron charge,  $M_S$  is the saturation magnetization of the magnetic layers,  $\mu_0$  is the permeability of vacuum, and  $t$  is the thickness of the free layer (FL).

The MTJ stack is shown in Fig. 1(a). The stack comprises (bottom to top) a field-biased synthetic antiferromagnetic layer (SAF), an insulating layer (I) and a ferromagnetic (FM) FL. The SAF layer comprises two FM layers separated by a non-magnetic spacer layer (NM). The FM layer next to the insulating layer is termed the PL of the MTJ stack. The use of SAF layer has been shown to reduce the stray field from the PL. To achieve the SAF, the two FM layers comprising the SAF are antiferromagnetically coupled with a two surface exchange energy  $\sigma$  of  $-1 \times 10^{-3} \text{ J/m}^2$ . The lower FM layer of the SAF stack is biased by a field of  $4 \times 10^5 \text{ A/m}$ . The magnetocrystalline anisotropy constant is assumed to be inversely proportional to the thickness of the FM layer  $t$ , as the interface coupling is decreased. Therefore, the thickness of the FL was chosen to be twice the thickness of the PL. The thickness of the FL is chosen to be 2 nm which shows the same trend as a magnetic layer of 2 nm thickness with a buffer layer of about 0.5 nm inserted. The thickness of 1 nm is chosen for all of the other FM layers. All the FM layers have a saturation magnetization  $M_S$  of  $1.3 \times 10^6 \text{ A/m}$  and an exchange stiffness constant  $A_{\text{Exch}}$  of  $3 \times 10^{-11} \text{ J/m}$ . The damping constant  $\alpha$  was set to 0.01 and the spin polarization  $\varepsilon$  of the PL to 0.7 to

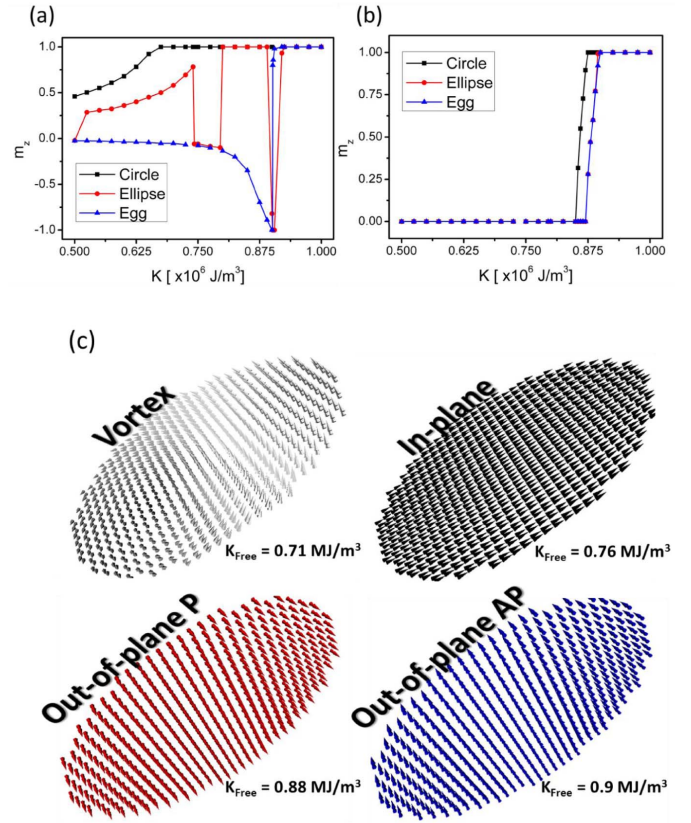


Fig. 2. Relaxed out-of-plane magnetization of the FL for a (a) stack and (b) single layer is shown. The final magnetization direction of the FL is shown in (c) for ellipses with magnetocrystalline anisotropy values of 0.71, 0.76, 0.88, and 0.9  $\text{MJ/m}^3$ .

simulate the efficiency of the tunnel junction. The cell mesh size is chosen to be  $1 \times 1 \times 1 \text{ nm}^3$  which is smaller than the exchange interaction length. Similar material parameters have been used in [11] and [12]. The Oersted field generated by the current flowing through the MTJ stack is neglected here.

## III. MAGNETOCRYSTALLINE ANISOTROPY INVESTIGATION

Three distinct shapes have been studied which are chosen due to their properties as completely symmetric (circular), partial symmetric (elliptical), and asymmetric as a mix between both structures (egg-shape). The top view of the structures investigated is shown in Fig. 1(b). The nominal area of the structures investigated is as follows: circular  $40 \times 40 \text{ nm}^2$ , elliptical  $60 \times 40 \text{ nm}^2$ , and the asymmetric elliptical (egg) shapes were varied between  $45$  and  $55 \times 40 \text{ nm}^2$ .

First, the normalized initial out-of-plane magnetization of the FL was set to +1 and then relaxed until the magnetization reaches its ground state. The normalized magnitude of the out-of-plane magnetization of the magnetic FL as a function of the magnetocrystalline anisotropy constant  $K$  is presented in Fig. 2(a). For reference, the normalized magnitude of the out-of-plane magnetization for a single layer with the same characteristic as the FL is shown in Fig. 2(b). The magnetocrystalline anisotropy constant for the FL was varied from 0.5 to 1  $\text{MJ/m}^3$ . As shown in Fig. 2(a), for the circular pMTJ, as the  $K$  value is reduced to  $0.67 \text{ MJ/m}^3$ , the relaxed magnetization state adopts an out-of-plane configuration.

Below this value, the magnetization adopts a vortex configuration. This confirms results which have been reported before [9]. For egg-shaped structure, we note that a  $K$  at  $0.9 \text{ MJ/m}^3$ , the magnetization adopts an opposite out-of-plane configuration. As the magnetocrystalline anisotropy  $K$  is further reduced, the magnetization of the FL adopts an in-plane configuration. For the elliptical structure, the relaxed state adopts an oscillating, positive and negative, out-of-plane configuration, as  $K$  is reduced. Below  $0.79 \text{ MJ/m}^3$ , the relaxed state adopts the in-plane configuration until it reaches below the  $K$  value of  $0.74 \text{ MJ/m}^3$ , where the magnetization adopts a vortex configuration. The magnetic configuration of the reference single layer is determined by the competition between the demagnetizing and the magnetocrystalline anisotropy fields. Interestingly, the magnetization changes its out-of-plane direction from out-of-plane anti-parallel (AP) to out-of-plane parallel P direction for the stack unlike the egg-shape from the single layer which moves in-plane.

For ellipse and egg-shaped structure, the single layer magnetization adopts an in-plane configuration at identically the same magnetocrystalline anisotropy constant  $K$ , whereas the circular structure retains its out-of-plane magnetization for even lower  $K$  values, as can be seen in Fig. 2(b). For the MTJ stack, however, the magnetization configuration exhibits a magnetization switch which can be assigned to the stray field from the SAF layer. For in-plane MTJ's the stray field of the SAF layer forms a closed loop which does not affect the magnetic FL [13], [14]. However, this is not the case for a perpendicular SAF layer where the magnetization of the PL affects the FL. For circular-shaped MTJ, the SAF stabilizes a third state between out-of-plane and in-plane configuration. This state is called vortex state which forms a circular in-plane magnetization around a center with out-of-plane magnetization consistent with previous simulations [9]. The SAF layer prevents the circular FL to fully turn in-plane. Interestingly, for egg-shaped MTJ's the magnetization of the FL switches at the same magnetocrystalline anisotropy as the single layer as shown in Fig. 2(b). The magnetization changes its out-of-plane direction from out-of-plane AP to out-of-plane parallel P direction for the stack unlike the egg-shape from the single layer which turns in-plane. This phenomenon gives proof that the SAF layer is affecting the FL in pMTJ stack different from in-plane MTJ systems [13], [14]. A further reduction of the magnetocrystalline anisotropy for egg-shaped MTJ also affects the strength of the SAF which reduces its intensity and the magnetization of the FL tilts slowly in-plane. Remarkably, the elliptical shape on the other side shows a pending out-of-plane magnetization between these two shapes dependent on the magnetocrystalline anisotropy  $K$ . This behavior must be related to the partly symmetric structure of the ellipse. The different magnetic states for elliptical-shaped FL can be seen in Fig. 2(c).

As for elliptical-shaped MTJ stack, the out-of-plane magnetization  $m_z$  is transiting between (+/-) out-of-plane magnetization as a function of  $K$ . We performed fast Fourier transform in order to investigate this phenomenon as the stable magnetization precession maybe dependent on the geometry and magnetocrystalline anisotropy. The fast Fourier transform

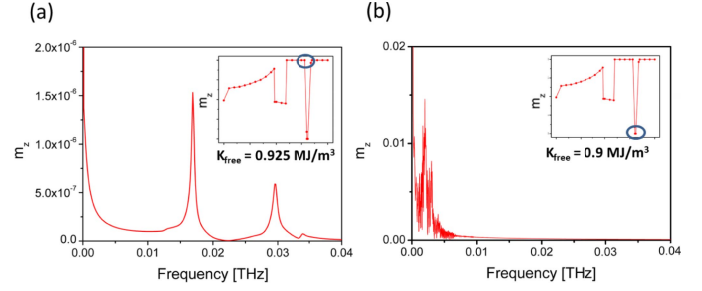


Fig. 3. Fast Fourier transform of the out-of-plane magnetization of elliptical FL for a magnetocrystalline anisotropy of (a)  $0.925 \text{ MJ/m}^3$  and (b)  $0.9 \text{ MJ/m}^3$ .

of the out-of-plane magnetization  $m_z$  for the relaxation process for different  $K$  values can be seen in Fig. 3(a) and (b) for AP and P configurations, respectively. For the AP case the frequencies are distinct with low magnitude of magnetization change. As for the P case, the magnitude of the magnetization significantly increases as the magnetization has to switch from AP to P. The frequencies are therefore lowered with a rather random distribution. This might be related to the symmetry axes and their ratio  $a/b$  from minor to major axis a completely different trend is observed. The collective magnetic configuration and stray field within the system enables the FL to have an out-of-plane magnetization at lower  $K$  for circular shape.

#### IV. CURRENT-INDUCED MAGNETIZATION SWITCHING

The current-induced magnetization switching via the STT phenomenon was investigated for circular and egg-shaped structures. The initial perpendicular magnetization  $m_z$  of 0.8 was chosen to introduce a symmetry breaking where the STT from the electrical current can act on the magnetization of the FL. When the magnetization of the polarizer and FL is aligned strictly P or AP, the STT effect will be nonexistent which follows a sine behavior of the out-of-plane magnetization angle according to (1). To obtain the 0.8 out-of-plane magnetization  $m_z$ , the magnetocrystalline anisotropy values for the circular and egg-shaped structure were  $0.6285$  and  $0.9015 \text{ MJ/m}^3$ . The initial state of the MTJ stack is in the AP state. A current pulse of 2 ns was applied along the negative  $z$ -direction to both stacks with a current density of  $1 \times 10^{11} \text{ J/m}^2$ . The pulse duration was chosen to be within the dynamics switching regime and to ensure that the magnetization of the FL switches completely.

Fig. 4 shows the out-of-plane magnetization dynamics of the FL as a function of simulation time. For the circular-shaped structure, we note that the magnetization switching occurs by a decreasing amplitude oscillatory behavior. The egg-shaped structure does not show any oscillation and there is an almost sharp change in magnetization configuration. We observe that the egg-shaped structure switches within 0.45 ns from  $m_z = 0.8$  to  $-0.8$  while the circular shape takes around 0.7 ns to switch. Two different dimensions for the circular stack are chosen to compare the effect of magnetic volume on the switching of the FL. The result shows that irrespective of the larger magnetic volume of the egg shape, the switching is still faster for the same current density applied. This is consistent with the fact that a constant current density is applied which

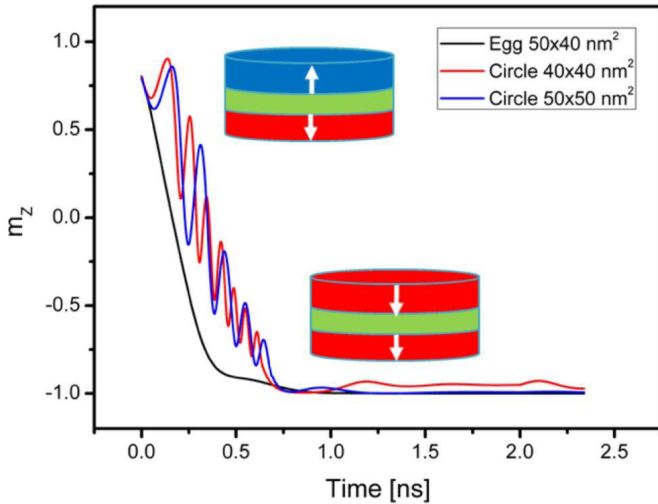


Fig. 4. Time-dependent perpendicular magnetization dynamics of the FL for an initial magnetization of  $m_z = 0.8$  versus time for different shapes and sizes.

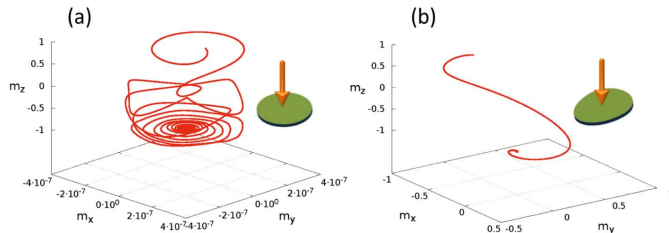


Fig. 5. Magnetization dynamics for (a) circular-shaped MTJ and (b) egg-shaped MTJ.

determines the switching time regardless of the cross-sectional area.

To gain a better understanding of the reversal process of the FL in circular and egg-shaped structure, we plotted the magnetization switching as a function of time for the MTJ stack. As shown in Fig. 5(a), the switching of the circular stack occurs via a precessional motion of the magnetic moments, whereas for the egg-shaped structure in Fig. 5(b) the magnetic moment in the FL does not undergo any oscillation. We extracted the spin configuration during the switching of pMTJ stacks. For the circular structure, we note that the switching of the FL is via the concentric reversal of the moments starting from the edge of the structure. As such, the switching of the core of the circular device leads to precessional motion of the spins. For the egg-shaped structure, we note that the reversal occurs from the smaller edge of the structure and propagates toward the larger edge, similar to the propagation of a domain wall (DW) as shown in Fig. 6.

To investigate the change of magnetization in further detail, we plotted the respective energies which are proportional to the magnetic fields. Fig. 7(a) and (c) show the time dependence of the exchange, uniaxial and demagnetization energy for a current density  $J$  of  $1 \times 10^{11}$  A/m<sup>2</sup>. The energy fluctuations for exchange, uniaxial, and demagnetization energies of the circular structure are on similar order of magnitudes and interact with each other which lead to different oscillations. This is further exemplified in the fast Fourier transform plot

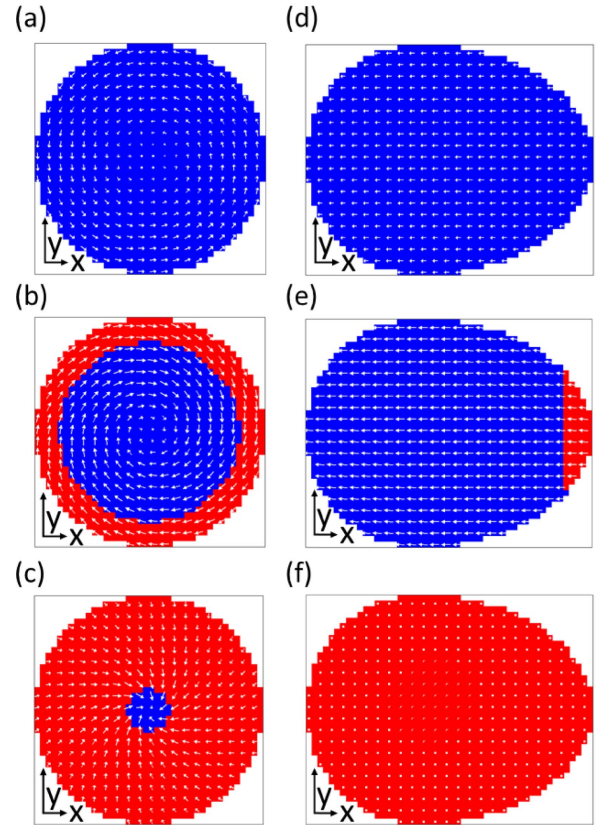


Fig. 6. (a) Initial magnetization state for the FL of the circular-shaped MTJ. (b) and (c) Intermediate magnetization states for the current-induced magnetization switching. (d)–(f) Magnetization states for the FL of the egg-shaped MTJs, respectively. The color code represents the out-of-plane magnetization where blue indicates the AP state with up magnetization and red indicates the P state with down magnetization.

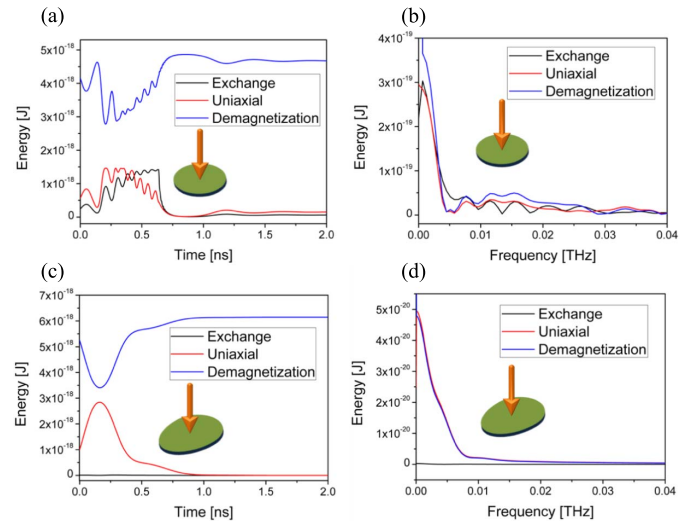


Fig. 7. (a) and (c) Time dependence for exchange, uniaxial, and demagnetization energy for (a) circular structure and (c) egg-shaped structure for a current density  $J$  of  $1 \times 10^{11}$  A/m<sup>2</sup>. (b) and (d) Frequency dependence for exchange, uniaxial, and demagnetization energy for (b) circular structure and (d) egg-shaped structure for a current density  $J$  of  $1 \times 10^{11}$  A/m<sup>2</sup>.

shown in Fig. 7(b). The demagnetizing energy change stands on the contrary to the uniaxial and exchange energies. The exchange energy oscillates at specific frequencies, whereas uniaxial and demagnetization energies change over a broader

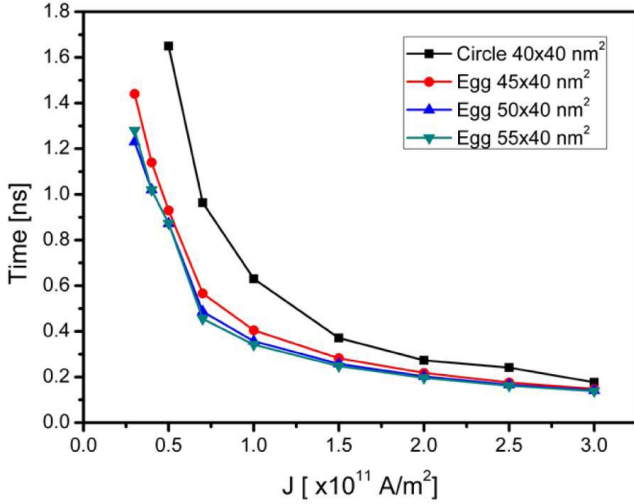


Fig. 8. Switching time depending on the current density for (a) circular and egg-shaped MTJs with initial perpendicular magnetization  $m_z = 0.8$  and magnetocrystalline anisotropies of  $1 \times 10^6$  J/m $^3$  and for (b) with same initial perpendicular magnetization and different ellipticities of the egg shape.

frequency range. This might be due to the vortex state exhibited by the circular structure at the beginning. Interestingly, the exchange energy of egg-shaped structure drops to nearly zero as shown in Fig. 7(c). This can be explained by the fact that the initial state of the egg-shaped structure has nearly parallel magnetic moments with  $m_z = 0.8$  out-of-plane magnetization which minimizes the exchange energy close to zero. Therefore, the uniaxial anisotropy energy increases until the magnetization is in-plane and drops again to a minimum when the magnetization is perpendicular again. The demagnetization energy drops at the beginning in the same way until the magnetization reaches the in-plane configuration and increases afterwards. Fig. 7(d) depicts the fast Fourier transform for egg-shaped structure. No induced frequency spectrum is observed which suggests that exchange energy is responsible for the oscillations.

Fig. 8 reveals the switching time dependence on the current density from AP to P state. We obtain for the same current densities lower switching times for the egg-shaped structure than those for the circular-shaped structure for  $m_z = 0.8$ . For a low-current density  $J$  of  $0.5 \times 10^{11}$  A/m $^2$  the switching time can be reduced by 47 %. In terms of reducing power consumption this reduction is remarkable because the egg-shaped structure exhibits a higher  $K$  value which leads to a higher current density. The switching time for the magnetization between  $m_z = 0.8$  and  $-0.8$  is following the trend given as [15]:

$$\tau \propto \frac{1}{\alpha J} \ln \frac{\theta}{\theta_0} \quad (2)$$

where  $\theta$  and  $\theta_0$  are the final and initial magnetization angles with respect to the  $z$ -direction. For the switching time, we kept the initial and final magnetization to  $m_z = \pm 0.8$  which is constant here. The inversely proportional trend from the current density to the switching time can be clearly seen in Fig. 8. The demagnetizing field is the main difference between the two structures. It should be noted that the effective

field here is also not the same for circular and egg-shaped MTJ because it includes the magnetocrystalline anisotropy and external magnetic effects. The stray field from the PL can be conceived as external magnetization field which is different for the two structures.

## V. DEMAGNETIZING FIELD INVESTIGATION

For a symmetric structure as the circular shape, the demagnetizing field is inside the plane and normal to the edges. The demagnetizing field can be written as

$$\vec{H}_D = (4\pi \vec{M}_S t y_0) \int_{-\infty}^{\infty} \frac{dx}{r^3} \quad (3)$$

where  $t$  is the thickness,  $y_0$  is the distance from the edge to the middle point, and  $r$  is the distance of the position to the middle point of the structure. The magnitude can be expressed by  $H_D = ((8\pi M_S t)/y_0)$ . For a more complex structure such as the elliptical or egg-shaped structure, the demagnetizing field has to be calculated analytically. It can be noted similar to the end of a bar magnet that the edge poles are situated at the edges of the long axis. For the egg-shaped structure, this is even more complicated because the long axis is not symmetrical which results in a disparate ratio of magnetic flux at the edge poles with a higher magnetic flux at the narrower edge. For any given geometry the demagnetizing field is given by

$$\vec{H}_D = 4\pi N \vec{M}_S \quad (4)$$

where  $N$  is the demagnetizing factor. The demagnetizing factor is a sum of the demagnetizing factors per coordinate ( $x, y, z$ )  $N = N_x + N_y + N_z$ . For elliptical shape, we can obtain [16]

$$N_x = \frac{\pi t}{4a} \left[ 1 - \frac{1}{4} \frac{a-b}{a} - \frac{3}{16} \left( \frac{a-b}{a} \right)^2 \right] \quad (5)$$

$$N_y = \frac{\pi t}{4a} \left[ 1 + \frac{5}{4} \frac{a-b}{a} + \frac{21}{16} \left( \frac{a-b}{a} \right)^2 \right] \quad (6)$$

$$N_z = 1 - N_x - N_y. \quad (7)$$

Factors  $a$  and  $b$  are the major and minor axis of the ellipse, respectively. For our ellipse with  $t = 2$  nm,  $a = 60$  nm, and  $b = 40$  nm, we obtain  $N_x = (\pi/120)(43/48)$ ,  $N_y = (\pi/120)(77/48)$ , and  $N_z = ((48 - \pi)/48)$ . The demagnetizing factor  $N_z$  is around 1 and much larger than the other two as expected for a very thin magnetization structure. Also, the fabrication of this structure is relatively simple. Unfortunately, this advantage is suspended if circular and egg-shaped structures are compared with a high  $K$  value of 1 MJ/m $^3$ . This underlines the importance of the initial spin configuration. The larger switching time can be explained by a lower torque which acts on the in-plane magnetization. For nearly perpendicular magnetization for  $K = 1$  MJ/m $^3$ , the initial torque is close to zero and starts growing with increased in-plane magnetization.

## VI. INVESTIGATION OF MATERIAL PARAMETERS ON CRITICAL SWITCHING CURRENT

The investigation of the current-induced magnetization switching in relation to the material parameters is

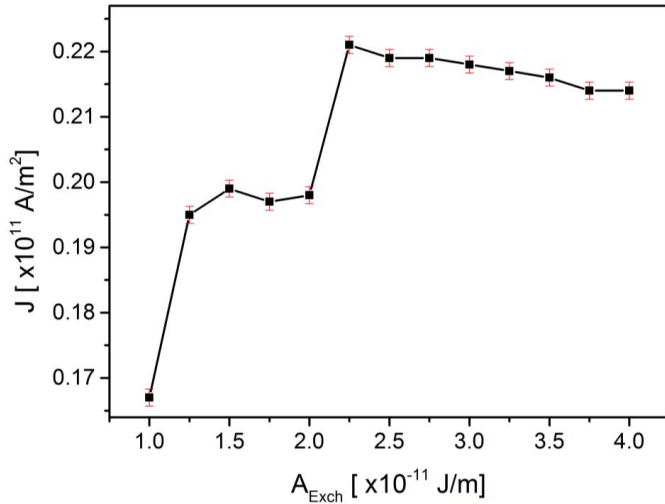


Fig. 9. Switching current as a function of the exchange constant of the FL for the egg-shaped structure with a unit magnetization  $m_z = 0.8$  to  $m_z = -0.8$ , a uniaxial constant  $K$  of  $0.9015 \times 10^6$  J/m<sup>3</sup> and a switching time of 2 ns.

of great interest for the successful implementation into devices [17]–[19]. The critical switching current density is given by the following relation [3], [20]:

$$J_C = \frac{2eaM_S H_{\text{eff}}}{\hbar e} \quad (8)$$

with  $H_{\text{eff}} = H_E + H_{\text{An}} + A_{\text{Exch}}k^2 + H_{\text{Dem}}$ , where  $H_E$  is the interlayer exchange field,  $H_{\text{An}} = (2K/M_S)$  the anisotropy field,  $k$  the spin-wave vector, and  $H_{\text{Dem}}$  denotes for the out-of-plane demagnetizing field.

The switching behavior of the asymmetric structure, egg-shaped, was investigated as a function of the exchange stiffness constant. The critical current density as a function of the exchange stiffness constant is shown in Fig. 9. The time for this magnetization reversal process from AP to P state has been fixed to 2 ns for a magnetization change of  $m_z = 0.8$  to  $-0.8$ .

The critical current density in a range of  $1.25$ – $2.25 \times 10^{-11}$  J/m from the exchange stiffness constant increases stepwise with a nearly constant current density above. The step can be explained due to an additional spin wave within the fixed time of 2 ns. The decrease in current density from exchange constants  $2.25$  to  $4 \times 10^{-11}$  J/m cannot be explained by (8) and must be attributed to the fixed simulation time. For the simulated structure an exchange constant of  $3 \times 10^{-11}$  J/m has been used which corresponds to a relatively stable current density of around  $0.216 \times 10^{11}$  A/m<sup>2</sup>.

The damping constant  $\alpha$  is also of great importance for the switching behavior as seen from (2) as well as from (8). A linear relationship is therefore expected for the critical current density as a function of the damping constant, as shown in Fig. 10.

In a range of 0.03–0.2 of the damping constant, a linear trend of the critical current density is observed. However, at lower damping constant an unexpected increase in current density is discovered. The fixed time leads to an artifact for low damping constant where the state of the spin wave is more crucial compared to larger damping constant.

The saturation magnetization is an intrinsic property of

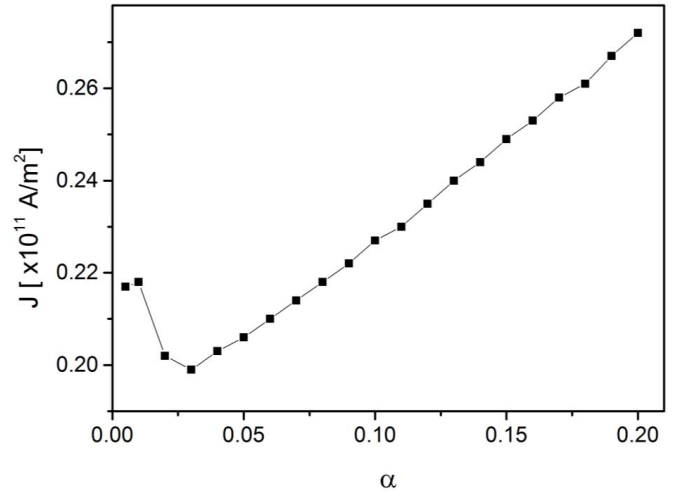


Fig. 10. Switching current as a function of the damping constant of the FL for the egg-shaped structure with a unit magnetization  $m_z = 0.8$  to  $m_z = -0.8$ , a uniaxial constant  $K$  of  $0.9015 \times 10^6$  J/m<sup>3</sup> and a switching time of 2 ns.

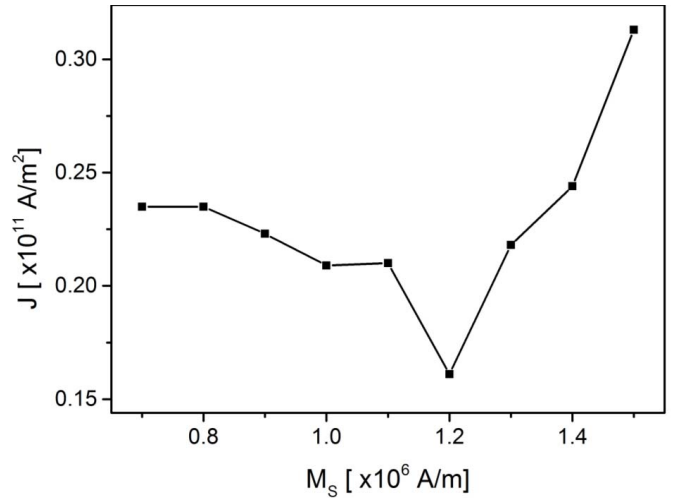


Fig. 11. Switching current as a function of the saturation magnetization of the FL for the egg-shaped structure with a unit magnetization  $m_z = 0.8$  to  $m_z = -0.8$ , a uniaxial constant  $K$  of  $0.9015 \times 10^6$  J/m<sup>3</sup> and a switching time of 2 ns.

the material which can be altered through the fabrication process. The behavior of critical performance characteristics such as the magnetization dynamics as a function of the saturation magnetization is of crucial interest for an engineering integration into practical device architecture. The critical magnetization switching current density as a function of the saturation magnetization is shown in Fig. 11.

The critical current density first decreases as a function of saturation magnetization with a minimum at  $0.161 \times 10^{11}$  A/m<sup>2</sup> for a saturation magnetization of  $1.2 \times 10^6$  A/m, and increases for larger saturation magnetization. The decrease in current density from 0.235 to  $0.161 \times 10^{11}$  A/m<sup>2</sup> cannot be explained by the anisotropy field decrease with increasing saturation magnetization. We rather believe that the lateral structure induces spin waves, because they lower the current density with increasing saturation magnetization. The maximum number of spin waves should be denoted at the saturation magnetization with the lowest critical current density. For saturation magnetization larger than  $1.2 \times 10^6$  A/m an increase in current density is observed as expected from (8).

## VII. CONCLUSION

We have performed micromagnetic simulations on representative pMTJ stacks with circular, elliptical, and egg-shaped cross section, to mimic the different lateral deformations. The results show that lateral defects greatly influence the magnetic stability. This leads to requiring larger perpendicular magnetocrystalline anisotropy to sustain the same magnetization state as the circular structures.

This can be explained by the symmetry breaking induced by the lateral defect in the MTJ.

## ACKNOWLEDGMENT

This work was supported in part by the Singapore National Research Foundation, Prime Minister's Office, through a Competitive Research Program (Non-volatile Magnetic Logic and Memory Integrated Circuit Devices) under Grant NRF-CRP9-2011-01 and an Industry-IHL Partnership Program Grant NRF2015-IIP001-001 and in part by a MOE-AcRF Tier 2 under Grant MOE 2013-T2-2-017. The support from an RIE2020 AME-Programmatic Grant (No. A1687b0033) is also acknowledged. W. S. Lee is a member of the Singapore Spintronics Consortium (SG-SPIN).

## REFERENCES

- [1] J. A. Katine, F. J. Albert, R. A. Buhrman, E. B. Myers, and D. C. Ralph, "Current-driven magnetization reversal and spin-wave excitations in Co/Cu/Co pillars," *Phys. Rev. Lett.*, vol. 84, no. 14, pp. 3149–3152, 2000.
- [2] S. S. P. Parkin *et al.*, "Giant tunnelling magnetoresistance at room temperature with MgO (100) tunnel barriers," *Nature Mater.*, vol. 3, pp. 862–867, Oct. 2004.
- [3] K. L. Wang, J. G. Alzate, and P. K. Amiri, "Low-power non-volatile spintronic memory: STT-RAM and beyond," *J. Phys. D, Appl. Phys.*, vol. 46, no. 7, p. 074003, 2013.
- [4] E. Chen *et al.*, "Advances and future prospects of spin-transfer torque random access memory," *IEEE Trans. Magn.*, vol. 46, no. 6, pp. 1873–1878, Jun. 2010.
- [5] M. Hatami, G. E. W. Bauer, Q. Zhang, and P. J. Kelly, "Thermal spin-transfer torque in magnetoelectronic devices," *Phys. Rev. Lett.*, vol. 99, no. 6, p. 066603, 2007.
- [6] D. Chiba, S. Fukami, K. Shimamura, N. Ishiwata, K. Kobayashi, and T. Ono, "Electrical control of the ferromagnetic phase transition in cobalt at room temperature," *Nature Mater.*, vol. 10, pp. 853–856, Oct. 2011.
- [7] M. Endo, S. Kanai, S. Ikeda, F. Matsukura, and H. Ohno, "Electric-field effects on thickness dependent magnetic anisotropy of sputtered MgO/Co<sub>40</sub>Fe<sub>40</sub>B<sub>20</sub>/Ta structures," *Appl. Phys. Lett.*, vol. 96, no. 21, p. 212503, 2010.
- [8] S. C. Oh *et al.*, "Improvement of writing margin in MRAM with novel shape," *J. Appl. Phys.*, vol. 97, no. 10, p. 10P509, 2005.
- [9] C.-Y. You and H. Kim, "Metastable Vortex state of perpendicular magnetic anisotropy free layer in spin transfer torque magnetic tunneling junctions," *J. Magn.*, vol. 18, no. 4, pp. 380–385, 2013.
- [10] *OOMMF Simulation*. Accessed: Jun. 2015. [Online]. Available: <http://math.nist.gov/oommf>
- [11] M. H. Jung, S. Park, C.-Y. You, and S. Yuasa, "Bias dependences of in-plane and out-of-plane spin-transfer torques in symmetric MgO-based magnetic tunnel junctions," *Phys. Rev. B, Condens. Matter*, vol. 81, no. 13, p. 134419, 2010.
- [12] C.-Y. You, J. Yoon, S.-Y. Park, S. Yuasa, and M.-H. Jung, "Magnetic noise spectra and spin transfer torque of a magnetic tunnel junction with an exchange biased synthetic ferrimagnetic reference layer," *Current Appl. Phys.*, vol. 11, no. 2, pp. e92–e94, 2011.
- [13] J. Hayakawa *et al.*, "Current-induced magnetization switching in MgO barrier magnetic tunnel junctions with CoFeB-based synthetic ferrimagnetic free layers," *IEEE Trans. Magn.*, vol. 44, no. 7, pp. 1962–1967, Jul. 2008.
- [14] W. C. Jeong, J. H. Park, G. H. Koh, G. T. Jeong, H. S. Jeong, and K. Kim, "Switching field distribution in magnetic tunnel junctions with a synthetic antiferromagnetic free layer," *J. Appl. Phys.*, vol. 97, no. 10, p. 10C905, 2005.
- [15] J. Z. Sun, "Spin-current interaction with a monodomain magnetic body: A model study," *Phys. Rev. B, Condens. Matter*, vol. 62, no. 1, pp. 570–578, 2000.
- [16] D. D. Tang, and Y.-J. Lee, *Magnetic Memory: Fundamentals and Technology*. Cambridge, U.K.: Cambridge Univ. Press, 2010.
- [17] C. Engel, S. Goolaup, F. Luo, and W. S. Lew, "Quantitative characterization of spin-orbit torques in Pt/Co/Pt/Co/Ta/BTO heterostructure on the magnetization azimuthal angle dependence," *Phys. Rev. B, Condens. Matter*, vol. 96, p. 054407, 2017.
- [18] M. Ramu, S. Goolaup, S. Krishnia, G. J. Lim, and W. S. Lew, "Spin orbit torque induced asymmetric depinning of chiral Néel domain wall in Co/Ni heterostructures," *Appl. Phys. Lett.*, vol. 110, p. 162402, 2017.
- [19] S. Li, S. Goolaup, J. Kwon, F. Luo, C. Engel, W. Gan, and W. S. Lew, "Deterministic spin orbit torque induced magnetization reversal in Pt/[Co/Ni]<sub>2</sub>/Ta structure," *Sci. Rep.*, vol. 7, p. 972, 2017.
- [20] S. M. Rezende, F. M. de Aguiar, and A. Azevedo, "Spin-wave theory for the dynamics induced by direct currents in magnetic multilayers," *Phys. Rev. Lett.*, vol. 94, no. 3, p. 037202, 2005.